surfaces

MDPI

Article

Tubular Wax Projections on Plant Epidermal Surfaces as Anti-Adhesive Coatings for Insects: A Numerical Modeling Approach

Stanislav N. Gorb, Elena V. Gorb * and Alexander E. Filippov

Functional Morphology and Biomechanics, Institute of Zoology, Kiel University, Am Botanischen Garten 9, 24098 Kiel, Germany; sgorb@zoologie.uni-kiel.de (S.N.G.); filippov_ae@yahoo.com (A.E.F.)
* Correspondence: egorb@zoologie.uni-kiel.de; Tel.: +49-431-8804509

Abstract

Three-dimensional (3D) epicuticular wax coverage on plant surfaces contributes to multifunctional surface properties, such as enhanced water repellence, reduced pathogen adherence, modified optical properties, and reduced insect adhesion. The diversity in wax projection morphology, size, abundance, and spatial arrangement among plant species results in a broad spectrum of anti-adhesive effects, reflecting both phylogenetic history and ecological function. This study presents a numerical model consisting of 3D tubular-shaped structures randomly deposited on a substrate and forming a highly porous layer. The simulations based on this model demonstrate a strong reduction in adhesion to the contacting insect adhesive pad. It is found that a structure formed by sufficiently long tubes, where the length is enough to support the tubes in space and build a porous 3D structure with a very low density, at relatively weak attraction to the underlying substrate, leads to the weakest adhesion. The model is constructed on the basis of our recent works combining discrete and continuous approaches in biological modeling. It mainly exploits the technique of the movable digital automata, allowing modeling of numerous numerically elastic cylinders that can be moved in 3D space, elastically collide with one another and with boundaries, and build self-consistent surface structures, which can be used to mimic nano- or microscale surface coverages of real plants.

Keywords: adhesion mechanics; anti-adhesive surface; epicuticular wax; plant–insect interactions; porous elastic structure; wax projection; 3D structure

Check for updates

Academic Editor: Maurice Brogly

Received: 23 February 2026
Revised: 30 March 2026
Accepted: 3 April 2026
Published: 8 April 2026

Copyright: © 2026 by the authors. Licensee MDPI, Basel, Switzerland. This article is an open access article distributed under the terms and conditions of the Creative Commons Attribution (CC BY) license.

1. Introduction

Plants interact constantly with arthropods in their environments, establishing relationships that range from mutualistic pollination to antagonistic herbivory. For locomotion, feeding, mating, and oviposition, insects rely on efficient attachment to plant surfaces—a capability largely mediated by specialized morphological and biochemical features of their tarsal attachment organs. These organs exploit combinations of claws, adhesive pads, and secreted fluids to generate sufficient contact area and adhesion forces even on complex surface geometries [1]. However, the evolutionary arms race between plants and herbivorous insects has driven plants to develop surface traits that diminish insect adhesion, serving as a physical defense against herbivorous insect pests and nectar robbers [1–5].

A ubiquitous and ecologically significant feature of aerial plant surfaces is the epicuticular wax layer—a hydrophobic film of long-chain aliphatic and cyclic hydrocarbons

and their derivatives that crystallizes on the outer cuticle [6–8]. Epicuticular wax projections vary greatly in their morphology, including plates, platelets, rodlets, tubules, filaments, etc., and range in size from less than one micrometer to several tens of micrometers [1,5,9–12]. These structures confer a set of multifunctional surface properties to plants, such as enhanced water repellence, reduced pathogen adherence, modified optical properties [6,7,13,14], and, importantly, reduced insect adhesion [1,15–20]. The diversity in crystal morphology, size, abundance, and spatial arrangement among plant species contributes to a broad spectrum of anti-adhesive effects, reflecting both phylogenetic history and ecological function [1,6,7,15,18,20–22].

Numerous experimental studies have demonstrated that plant surfaces covered with three-dimensional (3D) epicuticular waxes show significantly reduced insect attachment compared to smooth or wax-free surfaces [1]. Force measurements and traction experiments consistently reveal weaker adhesion and frictional forces for a wide range of insects, including beetles, flies, aphids, and stick insects, when tested on wax-covered plant surfaces. For example, surfaces with wax projections often decrease insect traction and pull-off forces by several folds relative to smooth controls. Importantly, this reduction is often correlated with crystal dimensions and density: larger and sparsely distributed crystals generally cause greater reduction in attachment strength [23]. These consistent observations across taxa underscore the functional effectiveness of 3D epicuticular waxes as physical anti-adhesive barriers.

Several mechanistic hypotheses have been proposed to explain how 3D plant waxes interfere with insect adhesion. The most widely supported mechanism is the roughness hypothesis, which posits that the nano- and microscopic topography created by wax projections drastically reduces the real contact area between the insect's adhesive pad and the substrate [4]. Adhesion and friction forces in biological systems are strongly dependent on intimate contact at the molecular level; when surface roughness exceeds certain critical dimensions relative to pad structures, insects cannot conform their soft adhesive tissues sufficiently, and adhesive forces decline sharply. Experimental and theoretical work supports this idea: critical roughness scales that prevent insect adhesion overlap with the typical size ranges of epicuticular wax projections [4,24–26].

In addition to geometric roughness, the contamination hypothesis suggests that wax projections, particularly those loosely bound to the cuticle, can detach and adhere to insect attachment organs, thereby impairing their adhesive function [1,4,25–29]. Detached projections or their fragments may lodge within the microstructures of adhesive pads, effectively creating a secondary rough layer on the pad surface that further reduces actual contact with subsequent substrates. This mechanism has been directly observed for certain plant species with fragile wax crystals and correlates with decreased attachment in insects [27–31].

Other mechanisms have been proposed, including the fluid-adsorption hypothesis, which suggests highly porous wax coverages can absorb the lipid-rich secretion that mediates wet adhesion in many insects, thereby weakening adhesive forces [4,32,33]. Finally, the wax-dissolving hypothesis posits that components of insect pad secretions may chemically interact with and dissolve parts of the wax projections, altering surface chemistry in a way that hinders adhesion. While evidence for this latter mechanism remains limited, it highlights the complex interplay of physical and chemical factors at the insect–plant interface.

Collectively, these mechanisms illustrate how 3D plant epicuticular waxes operate as multifaceted anti-adhesive surfaces shaped by millions of years of coevolution with insect appendages. Understanding these natural strategies not only deepens ecological insight into plant–insect interactions but also inspires biomimetic applications in agriculture and materials science aimed at reducing pest attachment through engineered surface topogra-

phies. This study was undertaken to understand how the geometry and arrangement of one particular type of wax projections alter the adhesion of plate-like structures similar to those of insect adhesive pads. We selected tubular wax projections, as they are present in numerous plant taxa (Figure 1), such as for example *Nelumbo nucifera*, *Aquilegia vulgaris*, *Chelidonium majus*, *Prunus domestica*, and *Eucalyptus gunnii*.

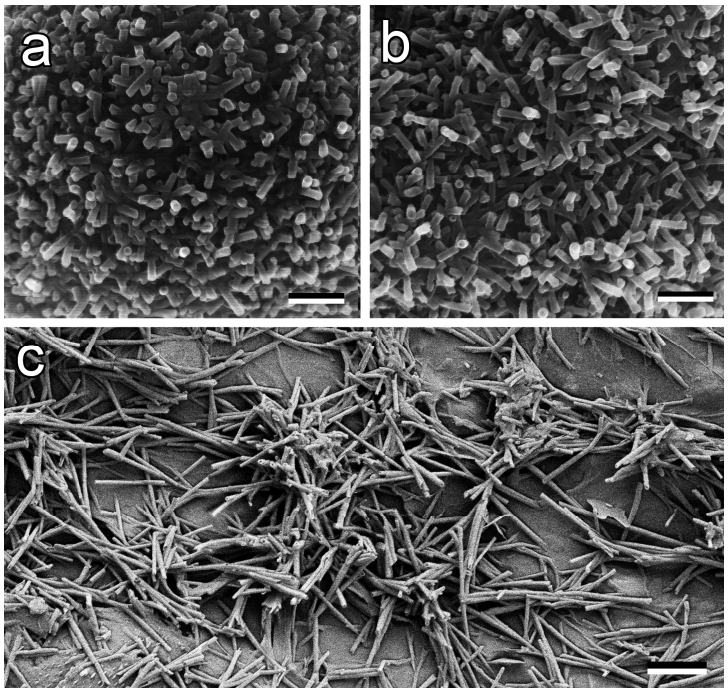


Figure 1. Scanning electron microscopy (SEM) micrographs of plant surfaces with tubular wax projections in the adaxial (upper) leaf side of *Aquilegia vulgaris* (**a**), *Chelidonium majus* (**b**), and *Eucalyptus globulus* (**c**). Scale bars: 1 μm (**a**,**b**); 2 μm (**c**). (**a**,**b**) from [20].

Using a numerical modeling approach, we generated surfaces covered by tubular structures of different aspect ratios in various arrangements on the surface (depending on the degree of their interactions with the neighboring tubes) and numerically probed their adhesiveness, which is dependent on their contact area with the approaching adhesive plate that simulated an insect adhesive pad. The model was constructed on the basis of our recent works combining discrete and continuous approaches in biological modeling [34]. It mainly exploits the technique of the movable digital automata, allowing modeling of numerous numerically elastic cylinders that can be moved in 3D space, elastically collide with one another and with boundaries, and build self-consistent surface structures, which can be used to mimic experimentally observable nanoscale surface coverages of real plants.

2. General Description of the Model

The system under consideration can be basically treated as a large number of 3D cylindrical shells, which mechanically mimic the wax tubes forming a complex porous (fractal) epicuticular plant coverage (see SEM images in Figure 1). Taking minimization of the numerical time consumption into account, it seems natural to create a simplified artificial model of every real tube using a set of more or less uniformly distributed nodes of cylindrical mesh (shell), which basically reproduces the form of the real tube. Having such a shell model in hand, one can turn on a mutual interaction of the tubes, add their interaction with a solid substrate, and solve a system with a relatively small number of dynamic equations to simulate sufficiently realistic behavior.

Observing the simulation results in dynamics, one can adjust all the interactions to reproduce rather realistic scenarios, where the objects would be allowed to collide and rotate in 3D space as elastic objects, interacting with boundaries and with the insect adhesive pad (later called the foot) when the latter is placed on the top of a system built using a large enough set of tubes. Our previous experience indicates that, in contrast to other methods of simulation, such an approach is less time-consuming (which normally happens for complex many-body systems) but reproduces reasonably realistic and practically interesting aspects of reality.

A number of examples of numerically generated systems for the problem under consideration are shown in the figures below. The construction of the tubes resembles the one applied in our previous studies [34]. Formally, the equations of motion are very compact and similar to the Newtonian ones:

$$m_i \partial \mathbf{v}_i / \partial t = -\partial H(\mathbf{x}_i, \mathbf{p}_i) / \partial \mathbf{p}_i = \mathbf{f}_i \quad (1)$$

where, as usual, the information about the system is contained in the structure of the Hamiltonian $H(\mathbf{x}_i, \mathbf{p}_i)$. From a mathematical point of view, the model describes a system of N particles represented by the vector radius $\mathbf{r}_i$, the momentum $\mathbf{p}_i$, and the interaction potential $U(|\mathbf{r}_i - \mathbf{r}_j|)$. Trial interaction between the nodes forming the mesh is a mutual repulsion. For example,

$$U_{repuls}(|\mathbf{r}_i - \mathbf{r}_j|) = C_{ij} \exp\{-[(\mathbf{r}_i - \mathbf{r}_j)/c_{ij}]^2\} \quad (2)$$

where C_{ij} define the magnitude, while c_{ij} are the radii of the repulsion. Notably, this repulsion does not allow different parts of the system to collide with one another. Besides, one needs a kind of "effective" attraction, which maintains the distances between the nodes close to their originally prescribed values:

$$U_{elastic}(\mathbf{r}_i - \mathbf{r}_j|) = K_{ij} \exp\{-[(\mathbf{r}_i - \mathbf{r}_j)/r_k]^2\}\{1 - [(\mathbf{r}_i - \mathbf{r}_j)/a_{ij}]^2\} \quad (3)$$

This two-valley potential automatically keeps the nodes inside the tube always connected to each other at the characteristic constant (close to original) distance a_{ij}. Such interaction provides the stability for the mechanical system and imparts effective longitudinal and lateral stiffness, which is provided by the proper choice of elastic constants [34].

Technically, the procedure was organized as follows. We created a set of initial coordinates for every tube and calculated mutual distances for all pairs of nodes a_{ij} in it. When the interaction denoted by Equation (3) was applied, it allowed the tube to move stably and rotate freely in 3D space as a mesoscopic "body". In principle, one can tune the elastic constants, making them different for different parts of any complex structure that is made up of a combination of simpler ones. In particular, one can connect a given number of segments, either stronger or weaker, to better adjust the properties of the real tube.

We have applied this in our previous works for objects combining a small number of different parts. However, here we mainly concentrated on a study of the system produced by a large number of practically equivalent tubes. Moreover, our goal here was to study regularly how the length (aspect ratio) of the tubes and their interaction with a solid bottom substrate, representing a plant epidermal surface, influence the resulting system behavior. In this case, it was even better to take all tubes as exact equivalents and study the general (statistical) properties of the relatively large system.

Moving in space, the system of elastically connected nodes dissipates energy because of mutual friction between them. Such dissipation spreads, particularly when the body collides with either potential energy relief or artificially organized external boundaries.

The boundaries lead to repulsion, deformation of every tube, and result in dissipation, depending on the mutual velocity of different nodes.

If the dissipation is included

$$f_i^v \sim \sum_{j=1}^{N} (v_i - v_j) exp[-[(r_i - r_j)/c_v]^2] \quad (4)$$

the complete system can be described by the set of equations:

$$m_i \partial \mathbf{v}_i / \partial t = -\partial H(\mathbf{x}_i, \mathbf{p}_i) / \partial \mathbf{p}_i = \mathbf{f}_i + \mathbf{f}_i^v \quad (5)$$

It certainly loses energy with time and finally stops, because its total moment of motion tends to zero, i.e., $m_i \sum_i d\mathbf{v}_i / \partial t \to 0$. Usually, this does not occur when the kinetic energy is produced by a source working outside the purely dynamic description. One can formally incorporate it into the model using an artificial energy source ξ_i^v (for example, the so-called "Langevin source" ξ_i^v [35]).

However, the present study represents a case where one can treat a random stochastic supply as negligibly weak and where the system tends to stay close to an equilibrium. In this case, the system self-organizes into a frozen final state with extremely slow kinetics, as described by Equation (5). Dissipation and nonlinearity of interactions, together with the boundary conditions, cause desirable evolution and self-organization of the system. Understanding of this led us to the following simulation procedure.

1. We started with a random (generally unstable) uniform average distribution of N tubes (all below $N = const. = 150$) having some random initial velocities and allowed them to interact and move according to the system in Equation (5).
2. When, due to dissipation, the kinetic energy of the system E_{kin} became less than some preliminary prescribed limit (let us say $E_{kin} < 0.01 E_{kin}|_{t=0}$), we stopped the routine and calculated all desired values (in particular, the total adhesion force) for a practically unmovable static system.
3. After this, we changed either the length of the tubes or the force of their attraction with the substrate and resumed the routine. This gave us some new values.

The results of such a simulation, recorded in the resumed step-by-step procedure, are presented in the figures below as well as in Supplementary Movies S1 and S2.

3. Numerical Results Obtained from the Model

The typical intermediate state caused by the procedure described above is shown in Figure 2a. The tubes are plotted using MATLAB-generated surfaces in 3D space (MatLab R2022a, The MathWorks Inc., Natick, MA, USA). They are colored according to the difference between the kinetic $E_{kin} = \sum_{i=1}^{N} \mathbf{p}_i^2 / 2m$ and potential $U_j = \sum_{i,j=1}^{N} U(|\mathbf{r}_i - \mathbf{r}_j|)$ energy of every individual segment in the standard "jet" colormap of MATLAB. Such colorization is rather informative, because it visually separates individual tubes, simultaneously providing information about the z-coordinate of a particular surface segment and the local absolute stress of deformed ones (due to changes in their U_j potential energy). One can directly see from a comparison between Figure 2a and Figure 2b that an extremely strong attraction was obtained between the tubes and the bottom substrate. For comparison, we also added Figure 2c, which reproduces a typical 3D configuration found for extremely short tubes having a length comparable to their diameter $L \approx D$.

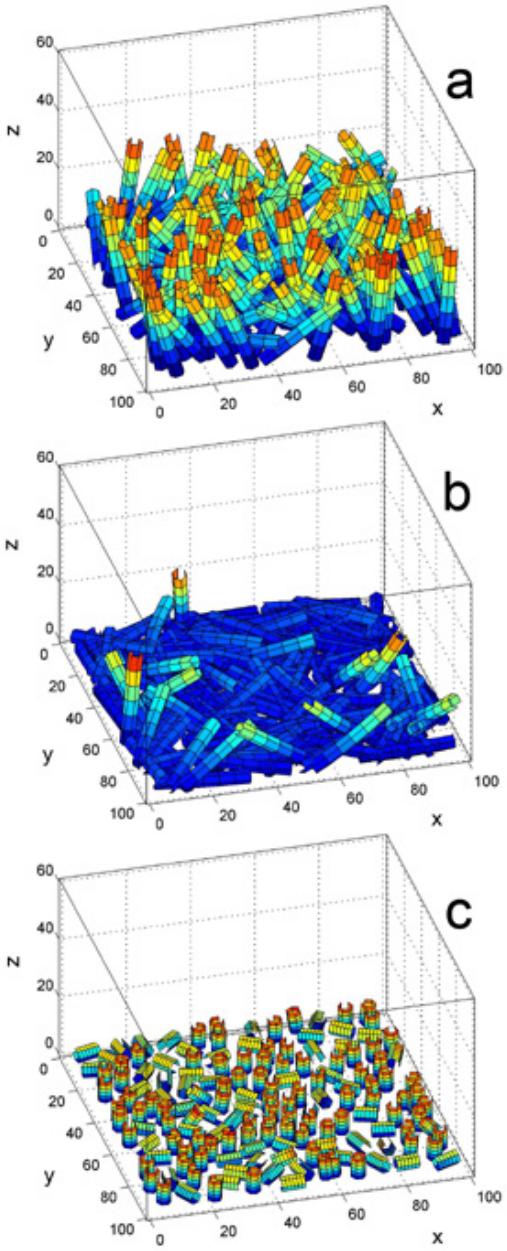


Figure 2. Typical result of random deposition of the tubes in 3D space, colored according to the difference between kinetic $E_{kin} = \sum_{i=1}^{N} \mathbf{p}_i^2/2m$ and potential $U_j = \sum_{i,j=1}^{N} U(|\mathbf{r}_i - \mathbf{r}_j|)$ energy for every individual segment in the standard "jet" colormap of MATLAB. The arrangement of tubes was obtained at weak (**a**) and extremely strong attraction (**b**) of the tubes to the substrate. (**c**) shows the results of deposition of very short tubes with lengths comparable to their diameters $L \approx D$.

The visualization of the simulation process should be accompanied by the quantitative (statistical) information extracted from the interactions incorporated into the model (Equation (5)). In particular, one can extract a histogram of the z-coordinate distribution of all the segments that make up the presented 3D structure at every realization of the model parameters (Figure 3a). Simultaneously, one can calculate the distribution of the adhesion force that influences every segment of each tube contacting the insect foot placed on top of the effective 3D surface (Figure 3c). How this calculation is carried out can be observed in the Supplementary Movies.

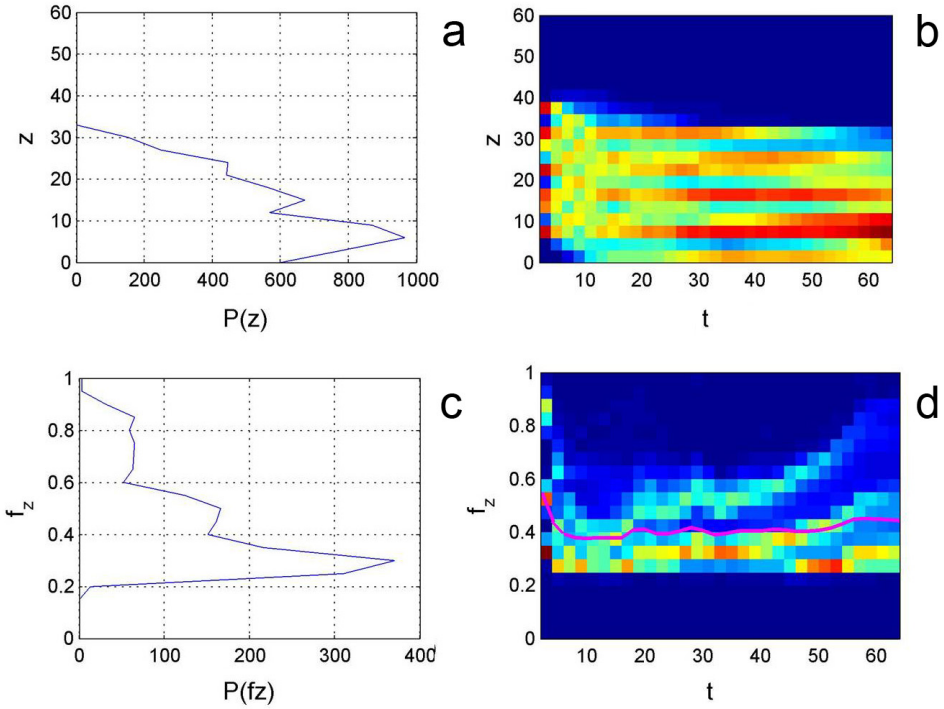


Figure 3. Instant intermediate distribution of the vertical coordinates z (**a**) and distribution of the local vertical force f_z (**c**) acting between the 3D structure and the planar surface placed on its top $Z = \max(z)$. Evolution over time of both distributions presented in (**a**,**c**) is reproduced in the time–space $\{t, z\}$ diagrams shown in (**b**,**d**), respectively.

Information about the evolution of these distributions over time can be collected and presented using artificial colors in time–space diagrams as it was done in static pictures. These diagrams (Figure 3b,d) recorded up to the same instant moment shown in Figure 3a,c, respectively, accompany the corresponding histograms of z-coordinate (Figure 3a) and vertical force f_z (Figure 3c).

As we already mentioned, the routine of the simulation was resumed every time we changed the model parameters. The complete evolution of the surfaces over time with regularly varied lengths of tubes is reproduced in Supplementary Movie S1. Static images of the important moments, for the convenience of the reader, are provided in Figure 4a–h. In this figure, each structure is shown at the stage when it is basically built, its kinetics is frozen, and quantitative data about the integral adhesion force are recorded. One can visually compare different structures formed at different tube lengths and qualitatively predict the expected integral adhesion. Figure 4i–p show eight static images of the advanced tube system configuration at varied attraction forces of the tubes to the underlying substrate (Supplementary Movie S2).

Effective upper surfaces of the 3D structure, found for every combination of tube length and attraction to the substrate, were calculated using the MATLAB scatter plot interpolation technique. In particular, this allowed restoration of the effective "footprints" of the contacts between the structures formed by each tube's special disposition and the insect foot placed horizontally on top of the 3D structure. Examples of such footprints are reproduced in Figure 5a,c,e. One can visually compare these footprints for different structures. It is especially interesting in Figure 5c demonstrating well-pronounced prints of the horizontally lying individual tubes.

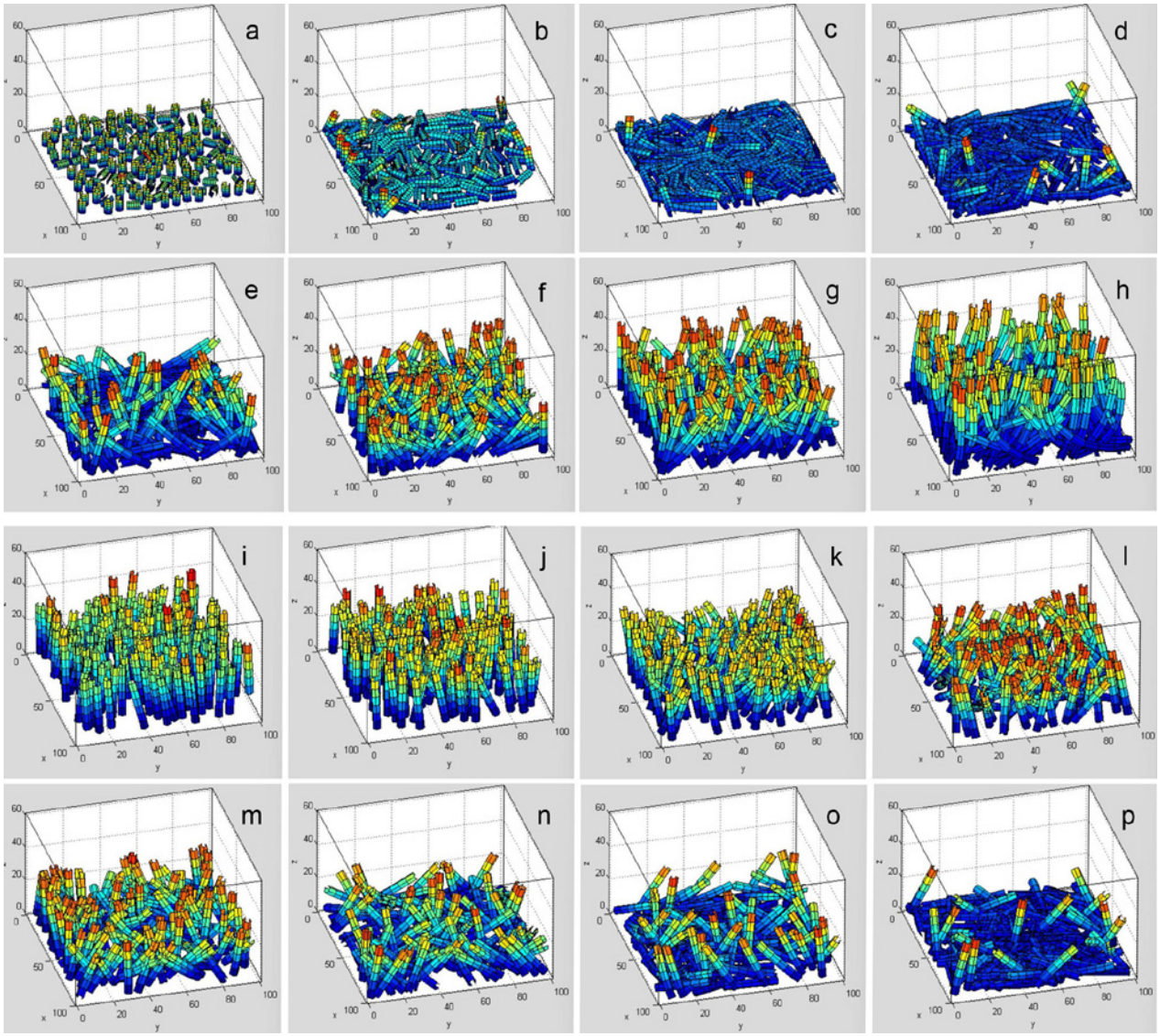


Figure 4. Complete evolution of the surfaces over time with different lengths of tubes and varied attraction forces of the tubes to the underlying substrate is presented in Supplementary Movies S1 and S2. (**a**–**h**) show eight static images of the advanced tube system configuration at varied tube lengths (Supplementary Movie S1). (**i**–**p**) show eight static images of the advanced tube system configuration at varied attraction forces of the tubes to the underlying substrate (Supplementary Movie S2). Each structure is shown at the stage when it is basically built, its kinetics are frozen, and quantitative data about the integral adhesion force are recorded. One can visually compare different structures formed at different tube lengths (**a**–**h**) or at different levels of attraction to the substrate (**i**–**p**) and qualitatively predict the expected integral adhesion. The lengths of the tubes range from one to twelve times their diameter. The interaction strength is from less than 0.1 to almost 1.2.

Using this model, one can also calculate the special correlation function $G(r - r') = \langle z(x, y)z(x', y') \rangle$ of every contact. Widths and depths of the maxima and minima provided us with clear information about the characteristic size of the voids in the real structure (which is actually strongly porous) and its anisotropy. In particular, the system in Figure 5c,d that demonstrates clear prints of the horizontally lying individual tubes shows rather pronounced anisotropy of the correlation function $G(r - r') = \langle z(x, y)z(x', y') \rangle$ as well.

From a biological point of view, the most important information can be extracted from the dependence of total (mean) adhesion on the length of the tubes making up a

highly porous 3D structure. This information is summarized in Figure 6. Interestingly, the structure formed by the sufficiently long tubes (where the length was sufficient to support the tubes in space and build a porous 3D structure having a very low density) showed relatively weak total adhesion for the system. In contrast, very short tubes of the dense 3D structure demonstrated the strongest adhesion to the insect foot.

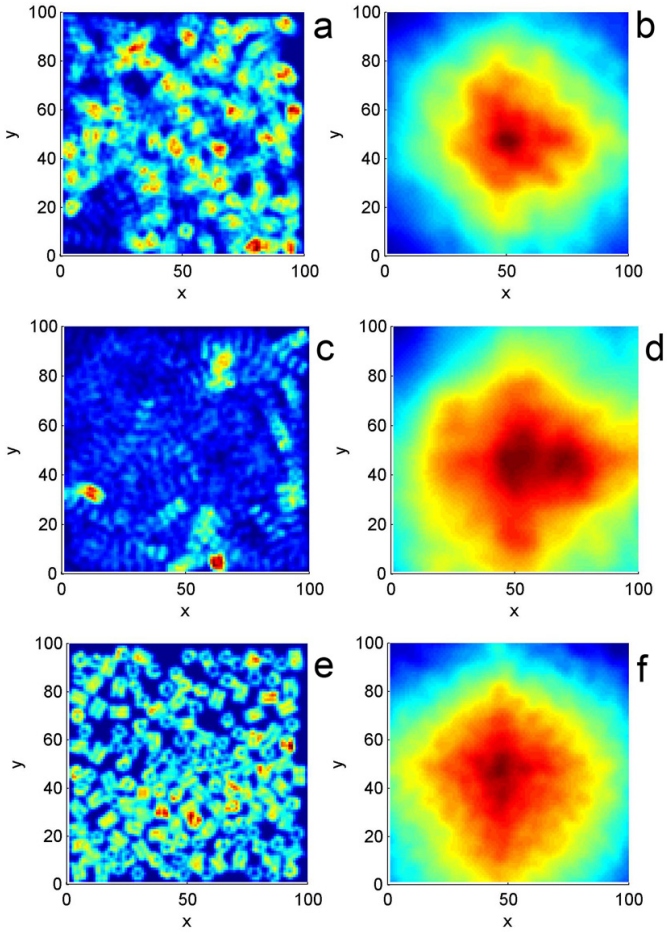


Figure 5. Examples of the insect "footprints" on the 3D wax structures. In (**a**,**c**,**e**), footprints of the contact between the upper surface of the 3D structure presented in Figure 2a–c, respectively, and a horizontal plane simulating an insect adhesive pad (foot) are shown. Corresponding correlation functions $G(r - r') = <z(x, y)z(x', y')>$ calculated for these surfaces are reproduced in (**b**,**d**,**f**).

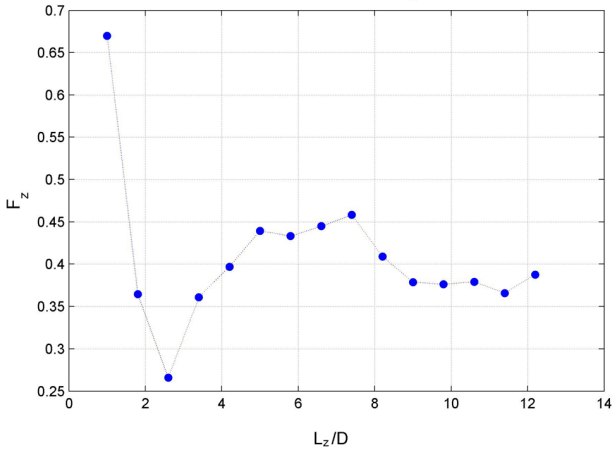


Figure 6. Total adhesion force F_z calculated for different lengths of tubes. L_z/D is length normalized to diameter. Dots are actual results of the numerical experiment. The line is a guide for eyes.

Dependence of the total (mean) adhesion force on the attraction force of the tubes with the underlying substrate is also very important (Figure 7). For this experiment, in order to obtain results comparable with the previous ones, we took the tubes of fixed intermediate length $L_z/D \simeq 5.5$. Three-dimensional structures with low density, which were formed at a relatively weak attraction to the substrate $f_{0z} \leq 0.4$, showed weak total adhesion to the insect foot in the corresponding limit. Much higher density of the structure, especially close to the substrate, was seen in the opposite limit. It caused stronger adhesion, as seen in the corresponding side of the curve.

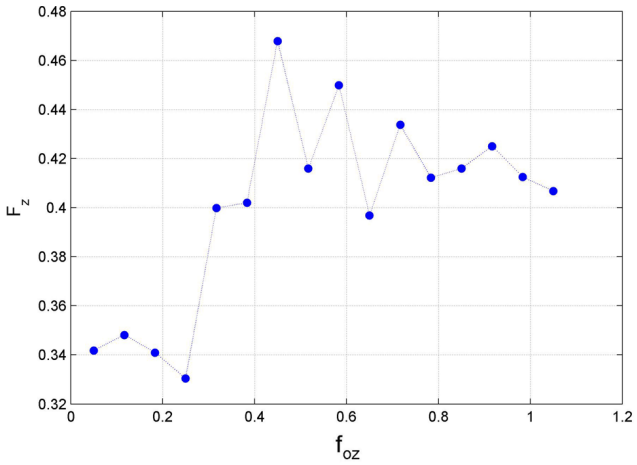


Figure 7. Total adhesion force F_z calculated for different attraction forces of tubes to the underlying substrate f_{0z}. Dots are actual results of the numerical experiment. The line is a guide for eyes.

4. Discussion

The porous layer of wax projections covering epidermal plant surfaces is generated by the numerical model. The model consists of wax tubes randomly disposed on a substrate. It is shown that it naturally reproduces the formation of the porous wax layer, which looks natural and provides reduced adhesion to the contacting insect foot placed on top of this layer. The numerical model is based on our recent works and mainly exploits the technique of the movable digital automata [34]. Numerically created elastic cylinders (tubes) can move in 3D space and collide with one another and their boundaries. They produce a 3D surface structure that visually mimics the coverage of real plants and gives reasonably correct numerical results. We studied their adhesive interactions with the flat plate simulating the insect adhesive pad.

4.1. Implications for the Anti-Adhesive Function of Plant Epicuticular Waxes

Plant epicuticular waxes are widely recognized as multifunctional surface coatings that play a crucial role in plant–environment interactions. Numerous experimental studies have demonstrated that wax-covered plant organs can significantly reduce attachment forces of insects [1,15–22,29], often leading to slipping or detachment. However, the mechanistic origin of these anti-adhesive properties remains complex, as wax layers exhibit pronounced structural diversity of highly porous 3D assemblies [9,36,37]. The numerical model presented in this work provides a physically transparent framework for interpreting anti-adhesive properties of waxy plant surfaces from a structural and mechanical point of view. By representing wax elements as elastic cylindrical tubes forming a porous, deformable layer, the model captures essential geometric and dynamical features observed in real plant wax coverage while remaining computationally tractable. Importantly, the model allows systematic variation of parameters that are difficult to control experimentally, such as effective wax projection length, stiffness, and interaction with the underlying

substrate. This makes it possible to directly relate the structural organization of the wax layer to the resulting adhesion forces acting on the insect's foot.

4.2. Porosity and Reduction of Real Contact Area

One of the central outcomes of the simulations is a strong dependence of total adhesion force on the spatial density and porosity of the tube-based layer. For sufficiently long tubes, the system self-organizes into an open, low-density 3D structure, where individual elements support one another and form a mechanically stable but highly porous network. In this regime, the effective upper surface of the 3D structure contacting the insect foot is fragmented and spatially heterogeneous, as demonstrated by the reconstructed footprints and their corresponding correlation functions.

From the perspective of contact mechanics, such a structure naturally leads to a strong reduction of real contact area [38–40]. Although the nominal contact area between the insect foot and the plant surface may be large, only a limited number of tube segments actually participate in load-bearing contact. This is fully consistent with experimental observations on waxy plant surfaces, where adhesion reduction is frequently attributed to diminished real contact due to surface roughness and nano- or microscale asperities [4,24,29]. The present model demonstrates that this effect does not require rigid roughness alone: a deformable, elastic, and dynamically assembled porous layer is sufficient to suppress adhesion even when individual elements are compliant.

In contrast, simulations with very short tubes show a collapse of the porous architecture into a much denser layer. In this limit, the upper surface of the 3D structure becomes more compact, and the number of contact points increases significantly. As a result, the total adhesion force rises sharply, in agreement with the intuitive expectation that denser surface coverage promotes stronger mechanical coupling between the foot and the substrate. This provides a natural explanation for why plant surfaces bearing distinct 3D wax structures often exhibit reduced adhesion compared to those with smoother or more compact wax films [30,31].

4.3. Mechanical Compliance and Energy Dissipation

Another important aspect revealed by the model is the role of mechanical compliance and energy dissipation within the wax layer. The elastic interactions between nodes, combined with dissipative forces, lead to a system that gradually relaxes into a mechanically stable, near-equilibrium configuration. During contact with the insect foot, local deformations of the tubes absorb part of the mechanical energy, while frictional dissipation between nodes prevents efficient force transmission across the layer.

This behavior closely parallels experimental findings, where epicuticular wax layers are described as mechanically fragile or are prone to deformation under load [26,29,41]. In such cases, adhesion is reduced not only because of the limited contact area, but also because applied forces are dissipated within the wax layer itself rather than being transmitted to the underlying rigid plant tissue. The model supports the idea that wax layers act as mechanical buffers, decoupling the animal attachment system from the solid substrate.

Importantly, the simulations show that excessive attraction of the tubes to the substrate leads to densification of the layer, especially near the underlying surface. This reduces the layer's ability to reorganize and deform, resulting in increased adhesion forces. From a biological point of view, this suggests that wax layers that are weakly bound to the plant cuticle or capable of partial detachment may be more effective in preventing adhesion. This finding is consistent with observations of easily removable wax projections in many plant species [28–31].

4.4. Anisotropy and Directional Effects

The reconstructed footprints and their correlation functions reveal that certain structural configurations, particularly those dominated by horizontally lying tubes, produce pronounced anisotropy in surface morphology. Such anisotropy may potentially have important biological implications. Directional dependence of adhesion and friction may affect the locomotion efficiency of insects depending on movement direction relative to surface microstructure, as previously shown for microstructural ridges (cuticular folds) of plants [42].

The present model demonstrates that such anisotropy can emerge naturally from the self-organization of flexible wax elements without imposing any predefined directional order. This suggests that plants may potentially exploit not only the presence of wax projections but also their statistical organization to create surfaces that are mechanically unfavorable for attachment in some preferred directions or under varying loading conditions.

4.5. Implications for Anti-Adhesive Strategies in Plants

Taken together, the results support the idea that anti-adhesive properties of plant waxes arise from a combination of geometric, mechanical, and dynamical factors. Rather than acting as a simple rough coating, wax coverages function as adaptive, self-organizing porous systems, whose macroscopic properties emerge from interactions at the mesoscopic scale. The numerical results indicate that optimal anti-adhesive performance is achieved in the regime where the wax elements are sufficiently long and weakly bound to the substrate, allowing the formation of a low-density, mechanically compliant network.

This finding aligns well with biological observations that many highly slippery plant surfaces bear elongated wax projections or even filaments forming 3D coverages [26,29,43]. Such structures minimize adhesion while remaining stable under environmental perturbations. Additionally, elongated wax projections with high aspect ratios may be easily broken, even under forces of single insect adhesive hairs, and contaminate insect adhesive organs [4,26,28–31]. Conversely, conditions that promote wax layer compaction (external load forces) or strong substrate binding may reduce the anti-adhesive effect, potentially explaining seasonal or developmental changes in plant surface properties [44].

4.6. Limitations and Outlook

While the present model intentionally simplifies the chemical and structural complexity of real epicuticular wax coverages, it captures key mechanical principles that are likely to be universal. The use of elastic cylindrical elements does not explicitly account for wax chemistry, crystallographic anisotropy, or fracture processes. Nevertheless, the robustness of the observed trends suggests that the anti-adhesive effect is primarily governed by mechanical organization rather than fine chemical details [45]. Future extensions of the model could include polydispersity of tube dimensions, different geometrical shapes of the structures, partial detachment or breakage of elements, and explicit coupling to more realistic animal attachment models. Such developments would further bridge the gap between numerical simulations and biological reality and may help to design bio-inspired anti-adhesive surfaces based on the same principles exploited by plants.

Supplementary Materials: The following supporting information can be downloaded at: https://www.mdpi.com/article/10.3390/surfaces9020037/s1. Supplementary Movie S1. Every part of the movie starts from the initial configuration with the array of vertical tubes randomly placed inside a square area of the underlying substrate. The tubes interact with one another, with side boundaries, and attract to the substrate, as described in the main text. Due to the complexity of the many-body problem, dynamic chaotization of the process develops and leads to the scenario that is directly seen in the movie. The difference between particular scenarios depends, among other parameters,

on an individual tube's length. This length is varied step by step from one section of the movie to another. Extremely short tubes mainly fall down to the substrate, while longer tubes collide with one another. This often prevents their complete falling and favors the formation of a complex (porous) 3D structure. Different behaviors of the system are associated with different total adhesion forces, which are calculated simultaneously with the process and are reproduced in the movie. Supplementary Movie S2. The same as in Movie 1, with variation in the attraction of the tubes to the substrate. One can see that after a critically strong attraction to the substrate, almost all the tubes fall down to the surface. This fall causes dense packing of the system and leads to a stronger mean adhesion force between the 3D structure and an imaginary horizontal plane placed on the top of the system.

Author Contributions: Conceptualization, S.N.G., E.V.G. and A.E.F.; Methodology, A.E.F.; Software, A.E.F.; Validation, S.N.G. and A.E.F.; Formal Analysis, S.N.G. and A.E.F.; Investigation, A.E.F.; Data Curation, S.N.G. and A.E.F.; Writing—Original Draft, S.N.G., E.V.G. and A.E.F.; Writing—Review and Editing, S.N.G., E.V.G. and A.E.F.; Visualization, S.N.G., E.V.G. and A.E.F.; Project Administration, S.N.G. All authors have read and agreed to the published version of the manuscript.

Funding: This research received no external funding.

Data Availability Statement: The original contributions presented in this study are included in the article and Supplementary Material.

Conflicts of Interest: The authors declare no conflict of interest.

Abbreviations

The following abbreviations are used in this manuscript:

SEM	Scanning electron microscopy
3D	Three-dimensional

References

1. Gorb, E.V.; Gorb, S.N. Anti-adhesive effects of plant wax coverage on insect attachment. *J. Exp. Bot.* **2017**, *68*, 5323–5337. [CrossRef]
2. Eigenbrode, S.D.; Espelie, K.E. Effects of plant epicuticular lipids on insect herbivores. *Annu. Rev. Entomol.* **1995**, *40*, 171–194. [CrossRef]
3. Eigenbrode, S.D.; Jetter, R. The effects of plant epicuticular waxy blooms on attachment and effectiveness of predatory insects. *Arth. Struct. Dev.* **2002**, *33*, 91–102. [CrossRef]
4. Gorb, E.V.; Gorb, S.N. Attachment ability of the beetle *Chrysolina fastuosa* on various plant surfaces. *Entomol. Exp. Appl.* **2002**, *105*, 13–28. [CrossRef]
5. Gorb, E.V.; Gorb, S.N. Anti-adhesive surfaces in plants and their biomimetic potential. In *Materials Design Insipred by Nature: Function through Inner Architecture*; Fratzl, P., Dunlop, J.W.C., Weinkamer, R., Eds.; The Royal Society of Chemistry: Cambridge, UK, 2013; pp. 282–309.
6. Jeffree, C.E. The fine structure of the plant cuticle. *Annu. Rev. Plant Physiol.* **1986**, *37*, 113–140.
7. Barthlott, W.; Neinhuis, C. Purity of the sacred lotus, or escape from contamination in biological surfaces. *Planta* **1997**, *202*, 1–8. [CrossRef]
8. Jeffree, C.E.; Baker, E.A.; Holloway, P.J. Ultrastructure and recrystallisation of plant epicuticular waxes. *New Phytol.* **1975**, *75*, 539–549. [CrossRef]
9. Barthlott, W.; Neinhuis, C.; Cutler, D.; Ditsch, F.; Meusel, I.; Theisen, I.; Wilhelmi, H. Classification and terminology of plant epicuticular waxes. *Bot. J. Linn. Soc.* **1998**, *126*, 237–260. [CrossRef]
10. Jetter, R.; Schäffer, S.; Riederer, M. Leaf cuticular waxes are arranged in chemically and mechanically distinct layers: Evidence from *Prunus laurocerasus* L. *Plant Cell Environ.* **2000**, *23*, 619–628. [CrossRef]
11. Jetter, R.; Riederer, M. In-vitro reconstitution of epicuticular wax crystals: Formation of tubular aggregates by long chain secondary alkanediols. *Bot. Acta* **1995**, *108*, 111–120. [CrossRef]
12. Jetter, R.; Kunst, L.; Samuels, A.L. Composition of plant cuticular waxes. In *Biology of the Plant Cuticle*; Riederer, M., Müller, C., Eds.; Blackwell Publishing: Oxford, UK, 2006.
13. Bargel, H.; Koch, K.; Cerman, Z.; Neinhuis, C. Structure-function relationships of the plant cuticle and cuticular waxes—A smart material? *Funct. Plant Biol.* **2006**, *33*, 893–910. [CrossRef]

14. Pfündel, E.E.; Agati, G.; Cerovuc, Z.G. Optical properties of plant surfaces. In *Biology of the Plant Cuticle*; Riederer, M., Müller, C., Eds.; Blackwell Publishing: Oxford, UK, 2006.
15. Stork, N.E. Slippery plant surfaces as defense mechanisms—A review. *Ecol. Entomol.* **1980**, *5*, 423–433.
16. Stork, N.E. Role of wax blooms in preventing attachment to brassicas by the mustard beetle, *Phaedon cochleariae*. *Entomol. Exp. Appl.* **1980**, *28*, 100–107. [CrossRef]
17. Stork, N.E. The form of plant waxes: A means preventing insect attachment? In *Insects and the Plant Surface*; Juniper, B.E., Southwood, T.R.E., Eds.; Edward Arnold: London, UK, 1986.
18. Juniper, B.E. Waxes on plant surfaces and their interactions with insects. In *Waxes: Chemistry, Molecular Biology and Functions*; Hamilton, R.J., Ed.; The Oily Press: Dundee, UK, 1995.
19. Eigenbrode, S.D.; Kabalo, N.N.; Stoner, K.A. Predation, behavior, and attachment by *Chrysoperla plorabunda* larvae on *Brassica oleracea* with different surface waxblooms. *Entomol. Exp. Appl.* **1999**, *90*, 225–235. [CrossRef]
20. Müller, C. Plant–insect interactions on cuticular surfaces. In *Biology of the Plant Cuticle*; Riederer, M., Müller, C., Eds.; Blackwell Publishing: Oxford, UK, 2006.
21. Bodnaryk, R.P. Epicuticular wax composition and insect resistance in *Brassica oleracea*. *Phytochemistry* **1992**, *31*, 2759–2766.
22. Brennan, M.; Weinbaum, S.A. Epicuticular wax and insect attachment: A comparative study of waxy and wax-deficient plants. *J. Entomol. Sci.* **2001**, *36*, 32–41.
23. Gorb, E.V.; Böhm, S.; Jacky, N.; Maier, L.-P.; Dening, K.; Pechook, S.; Pokroy, B.; Gorb, S.N. Insect attachment on crystalline bioinspired wax surfaces formed by alkanes of varying chain lengths. *Beilstein J. Nanotechnol.* **2014**, *5*, 1031–1041. [CrossRef]
24. Scholz, I.; Bückins, M.; Dolge, L.; Erlinghagen, T.; Weth, A.; Hischen, F.; Mayer, J.; Hoffmann, S.; Riederer, M.; Riedel, M.; et al. Slippery surfaces of pitcher plants: *Nepenthes* wax crystals minimize insect attachment via microscopic surface roughness. *J. Exp. Biol.* **2010**, *213*, 1115–1125. [CrossRef]
25. Borodich, F.M.; Gao, Z.; Gorb, E.V.; Gorb, S.N.; Jin, X. Wax protrusions on anti-adhesive plant surfaces and their interactions with insect adhesive pads: A mechanical interpretation. *Biomimetics* **2024**, *9*, 442. [CrossRef]
26. Borodich, F.M.; Gorb, E.V.; Gorb, S.N. Fracture behaviour of plant epicuticular wax crystals and its role in preventing insect attachment: A theoretical approach. *Appl. Phys. A* **2010**, *100*, 63–71. [CrossRef]
27. Juniper, B.E.; Burras, J.K. How pitcher plant trap insects. *New Sci.* **1962**, *269*, 75–77.
28. Gaume, L.; Perret, P.; Gorb, E.V.; Gorb, S.N.; Labat, J.J.; Rowe, N. How do plant waxes cause flies to slide? Experimental tests of wax-based trapping mechanisms in three pitfall carnivorous plants. *Arth. Struct. Dev.* **2004**, *33*, 103–111. [CrossRef]
29. Gorb, E.V.; Haas, K.; Henrich, A.; Enders, S.; Barbakadze, N.; Gorb, S.N. Composite structure of the crystalline epicuticular wax layer of the slippery zone in the pitchers of the carnivorous plant *Nepenthes alata* and its effect on insect attachment. *J. Exp. Biol.* **2005**, *208*, 4651–4662. [CrossRef]
30. Gorb, E.V.; Gorb, S.N. Do plant waxes make insect attachment structures dirty? Experimental evidence for the contamination hypothesis. In *Ecology and Biomechanics: A Mechanical Approach to the Ecology of Animals and Plants*; Herrel, A., Speck, T., Rowe, N.P., Eds.; CRC Press: Boca Raton, FL, USA, 2006; pp. 147–162.
31. Gorb, E.V.; Gorb, S.N. Insect attachment on waxy plant surfaces: The effect of pad contamination by different waxes. *Beilstein J. Nanotechnol.* **2024**, *15*, 385–395. [CrossRef] [PubMed]
32. Gorb, E.V.; Lemke, W.; Gorb, S.N. Porous substrate affects a subsequent attachment ability of the beetle *Harmonia axyridis* (Coleoptera, Coccinellidae). *J. R. Soc. Interface* **2019**, *16*, 20180696. [CrossRef]
33. Gorb, E.V.; Hofmann, P.; Filippov, A.E.; Gorb, S.N. Oil absorbing ability of three-dimensional epicuticular wax coverages in plants. *Sci. Rep.* **2017**, *7*, 45483. [CrossRef] [PubMed]
34. Filippov, A.E.; Gorb, S.N. *Combined Discrete and Continual Approaches in Biological Modelling*; Springer: Cham, Switzerland, 2020.
35. Langevin, P. Sur la théorie du mouvement brownien [On the Theory of Brownian Motion]. *C. R. Acad. Sci.* **1908**, *146*, 530–533.
36. Meusel, I.; Neinhuis, C.; Markstadter, C.; Barthlott, W. Ultrastructure, chemical composition, and recrystallization of epicuticular waxes: Transversely ridged rodlets. *Can. J. Bot.* **1999**, *77*, 706–720.
37. Meusel, I.; Neinhuis, C.; Markstadter, C.; Barthlott, W. Chemical composition and recrystallization of epicuticular waxes: Coiled rodlets and tubules. *Plant Biol.* **2000**, *2*, 462–470. [CrossRef]
38. Fuller, K.N.G.; Tabor, D. The effect of surface roughness on the adhesion of elastic solids. *Proc. R. Soc. A* **1975**, *345*, 327–342. [CrossRef]
39. Persson, B.N.J.; Gorb, S.N. The effect of surface roughness on the adhesion of elastic plates with application to biological systems. *J. Chem. Phys.* **2003**, *119*, 11437–11444. [CrossRef]
40. Kovalev, A.; Filippov, A.E.; Gorb, S.N. Critical roughness in animal hairy adhesive pads: A numerical modeling approach. *Bioinspir. Biomim.* **2018**, *13*, 66004. [CrossRef]
41. Gorb, E.V.; Gorb, S.N. Frictional properties of flower stems in the plant *Hippeastrum reginae* (Amaryllidaceae). *Appl. Phys. A* **2020**, *126*, 549. [CrossRef]

42. Voigt, D.; Schweikart, A.; Fery, A.; Gorb, S.N. Leaf beetle attachment on wrinkles: Isotropic friction on anisotropic surfaces. *J. Exp. Biol.* **2012**, *215*, 1975–1982. [CrossRef]
43. Oelschlägel, B.; Gorb, S.N.; Wanke, S.; Neinhuis, C. Structure and biomechanics of trapping flower trichomes and their role in the pollination biology of *Aristolochia* plants (Aristolochiaceae). *New Phytol.* **2009**, *184*, 988–1002. [CrossRef]
44. Neinhuis, C.; Barthlott, W. Seasonal changes of leaf surface contamination in beech, oak, and ginkgo in relation to leaf micromorphology and wettability. *New Phytol.* **1998**, *138*, 91–98. [CrossRef]
45. England, M.W.; Sato, T.; Yagihashi, M.; Hozumi, A.; Gorb, S.N.; Gorb, E.V. Surface roughness rather than surface chemistry essentially affects insect adhesion. *Beilstein J. Nanotechnol.* **2016**, *7*, 1471–1479. [CrossRef] [PubMed]

Disclaimer/Publisher's Note: The statements, opinions and data contained in all publications are solely those of the individual author(s) and contributor(s) and not of MDPI and/or the editor(s). MDPI and/or the editor(s) disclaim responsibility for any injury to people or property resulting from any ideas, methods, instructions or products referred to in the content.